BBA - Proteins and Proteomics 1873 (2025) 141050

Contents lists available at ScienceDirect

BBA - Proteins and Proteomics

journal homepage: www.elsevier.com/locate/bbapap

Structure and functional studies of Avt1, a novel peptide from the sea anemone *Aulactinia veratra*

Renad A. Albar [a], Hayden L. Smith [b], Karoline Sanches [a], Dorothy C.C. Wai [a], Muhammad Umair Naseem [c], Tibor G. Szanto [c], Gyorgy Panyi [c], Peter J. Prentis [b,d], Raymond S. Norton [a,e,*]

[a] Medicinal Chemistry, Monash Institute of Pharmaceutical Sciences, Monash University, Parkville, VIC 3052, Australia
[b] School of Biology and Environmental Science, Faculty of Science, Queensland University of Technology, Brisbane, QLD 4000, Australia
[c] Department of Biophysics and Cell Biology, Faculty of Medicine, University of Debrecen, Debrecen 4032, Hungary
[d] Centre for Agriculture and the Bioeconomy, Queensland University of Technology, Brisbane, QLD 4000, Australia
[e] ARC Centre for Fragment-Based Design, Monash University, Parkville, VIC 3052, Australia

ARTICLE INFO

Keywords:
Sea anemone
Cysteine-rich peptide
Ion channels
NMR spectroscopy
ICK fold

ABSTRACT

Sea anemones are a rich source of peptide toxins spanning a diverse range of biological activities, typically targeting proteins such as ion channels, receptors and transporters. These peptide toxins and their analogues are usually highly stable and selective for their molecular targets, rendering them of interest as molecular tools, insecticides and therapeutics. Recent transcriptomic and proteomic analyses of the sea anemone *Aulactinia veratra* identified a novel 28-residue peptide, designated Avt1. Avt1 was produced using solid-phase peptide synthesis, followed by oxidative folding and purification of the folded peptide using reversed-phase high-performance liquid chromatography. The liquid chromatography-mass spectrometry profile of synthetic Avt1 showed a pure peak with molecular mass 6 Da less than that of the reduced form of the peptide, indicating the successful formation of three disulfide bonds. The solution structure determined by NMR revealed that Avt1 adopts an inhibitor cystine knot (ICK) fold, in which a ring is formed by two disulfide bonds with a third disulfide penetrating the ring to create the pseudo-knot. This structure provides ICK peptides with high structural, thermal and proteolytic stability. Consistent with its ICK structure, Avt1 was resistant to proteolysis by trypsin, chymotrypsin and pepsin, although it was not a trypsin inhibitor. Avt1 at 100 nM showed no activity in patch–clamp electrophysiological assays against several mammalian voltage-gated ion channels, but has structural features similar to toxins targeting insect sodium ion channels. Although sequence homologues of Avt1 are found in a number of sea anemones, this is the first representative of this family to be characterised structurally and functionally.

1. Introduction

Sea anemones are ancient venomous marine animals belonging to the phylum Cnidaria, class Anthozoa, and order Actiniaria. A distinctive characteristic of cnidarians is the presence of numerous specialised stinging cells called nematocytes that are found mainly in tentacles but are distributed throughout the animal body. The nematocysts contain a complex venom discharged upon chemical or mechanical stimulation to capture prey and/or defend against predators [1–3]. The venoms of sea anemones are rich sources of biologically active compounds, including disulfide-rich peptides [4–8]. These peptides are potentially valuable molecular research tools and therapeutic leads as they selectively target various ion channels and receptors [9–12], while others exhibit antimicrobial, insecticidal and haemolytic properties [13–18]. Several venom-derived drugs are clinically approved to treat diseases, such as hypertension, diabetes mellitus, severe chronic pain, and myocardial infarction [19–23]. ShK-186 (Dalazatide) [24], based on the sea anemone toxin ShK [10,25], is currently in clinical trials as a new treatment for autoimmune diseases [26].

In recent years, genomic, transcriptomic, and proteomic analyses

* Corresponding author at: Medicinal Chemistry, Monash Institute of Pharmaceutical Sciences, Monash University, 381 Royal Parade, Parkville, VIC 3052, Australia.
E-mail address: ray.norton@monash.edu (R.S. Norton).

https://doi.org/10.1016/j.bbapap.2024.141050
Received 31 July 2024; Received in revised form 25 September 2024; Accepted 27 September 2024
Available online 30 September 2024

with advanced bioinformatic analyses have been widely utilised to investigate the molecular diversity of venom components, identifying many novel peptide sequences from sea anemones [27–33]. However, it remains a significant challenge to identify the target(s) of these peptides, as many display little or no activity against a range of characterised ion channels and receptors, and their endogenous functions are yet to be determined [34–39]. Techniques such as mass spectrometry imaging (MALDI–MSI) can potentially determine the tissue distribution of peptides, which can improve our understanding of their likely functions [40,41], as in the case of the predatory Kv PHAB toxins [42].

The sea anemone *Aulactinia veratra* (also known as the green snakelocks anemone), in the family Actinidae, is distributed widely in waters around the west, south, and east coasts of Australia and in New Zealand. It was reported that human contact with this sea anemone causes severe skin allergic reactions and lesions that take weeks to heal [43]. In the course of unpublished transcriptomic and proteomic studies [44] of *Aulactinia veratra* we identified a novel 28 amino acid peptide with three disulfide bonds in the milked venom. This peptide was designated U-AITx-Avt1 according to the nomenclature proposed by Oliveira et al. [45], but the short name Avt1 will be used here. In this study, Avt1 was synthesised using solid-phase methods and its solution structure determined using nuclear magnetic resonance (NMR) spectroscopy. In addition, its biological activities, including effects on a range of mammalian ion channels, resistance against proteolytic enzymes and haemolytic activity, were investigated.

2. Materials and methods

2.1. Identification of U-AITX-Avt1 (Avt1)

The putative toxin, Avt1, was identified in the previously assembled transcriptome for *Aulactinia veratra* [44]. The Avt1 sequence was then used to search assembled transcriptomes in several actiniarian species (11 actinioidean, seven metridioidean and two edwardsioidean species; Table S1) [44,46–48] for homologous sequences with a signal peptide and a significant match (*P*-value ≤1.0e-6) to the Avt1 amino acid sequence using Blast+ [49]. Sequences were filtered to ensure the presence of the canonical KR cleavage site preceding the mature peptide, a 6-cysteine framework, and a mature peptide length of 28 residues.

Further validation of Avt1 was obtained from the secreted venom proteome using previously established protocols [3,41,50]. Briefly, secreted venom was desalted using Biotech CE Tubing (MWCO: 100–500 Da; Spectrum Laboratories, Inc.), then reduced and alkylated using dithiothreitol (10 mM) and iodoacetamide (40 mM), respectively, before overnight tryptic digestion at 37 °C. A SCX resin (Empore) Stagetip was used for the desalting digest, before resuspension in a mass spectrometry (MS) buffer (2% acetonitrile, 0.1% formic acid) containing indexed retention time peptides. Peptide spectra were obtained on a TripleTOF 5600+ mass spectrometer (Sciex), and raw data were matched to the transcriptome using ProteinPilot (v5.0) and Skyline (v23.1) to search for high confidence (conf ≥95 and 1% FDR) peptide matches for the Avt1 sequence.

2.2. Peptide synthesis

Avt1 peptide was synthesised on an automated peptide synthesiser 3 (PS3; Protein Technologies Inc.) using the standard Fmoc strategy. Chlorotrityl chloride (CTC) resin (0.3–0.8 mmol/g, 200–400 mesh) was used to yield a C-terminal carboxylic acid peptide. Coupling reactions were carried out for 50 min and utilised mixtures of three equivalents of Fmoc-amino acid, three equivalents of O-(1H-6-chlorobenzotriazole1-yl)-1,1,3,3-tetramethyluronium hexafluorophosphate (HCTU) and 7% N,N-diisopropylethylamine (DIPEA) in *N*,*N*-dimethylformamide (DMF). After each coupling reaction, 20% piperidine in DMF was used to remove the Fmoc protecting group by agitating the resin in the piperidine solution twice for 5 min, followed by three washes with DMF. The complete peptide-containing resin was washed three times with DMF, methanol, and diethyl ether separately and then dried under a vacuum. Peptide was cleaved from the resin with simultaneous removal of side chain protecting groups using a cleavage mixture containing 92.3% trifluoroacetic acid (TFA), 1.2% 1,2-ethanedithiol (EDT), 1.2% triisopropylsilane (TIPS), 2.5% thioanisole and 2.8% H_2O, incubated with agitation for 3 h at room temperature. The mixture was then filtered to separate the peptide from the resin, and TFA was removed using a nitrogen stream. The crude peptide was precipitated and washed three times with cold diethyl ether, dissolved in 50% acetonitrile in H_2O and then lyophilised.

2.3. Reversed-phase high-performance liquid chromatography (RP-HPLC)

The crude peptide was resuspended in 95% buffer A (0.1% TFA in H_2O) and 5% buffer B (0.1% TFA in acetonitrile), filtered with a 0.22 μm syringe filter, and loaded onto a Vydac C18 column (250 × 4.6 mm, particle size 5 μm) operating on an Agilent 1260 Infinity II liquid chromatography system. The peptide was eluted using a flow rate of 4 mL/min and a linear gradient of 5–85% buffer B over 50 min. Collected fractions were analysed by liquid chromatography–mass spectrometry (LC-MS) for identity and purity on a Shimadzu 2020 LC − MS fitted with a Phenomenex Luna C8 reverse-phase column (100 × 2.0 mm, 3 μm,100 Å), using a gradient of 0–80% buffer B (buffer A: 0.05% TFA in H_2O) and buffer B (0.05% TFA in acetonitrile) at a flow rate of 0.2 mL/min over 15 min, with absorbance monitored at 220 nm. Fractions containing pure reduced peptide (>95%) were lyophilised and stored at −20 °C.

2.4. Oxidative refolding

The purified reduced peptide was dissolved in an oxidation buffer containing 50 mM Tris pH 8.0, 0.1 mM reduced glutathione (GSH), and 0.2 mM oxidised glutathione (GSSG) to a final peptide concentration of 0.1 mM (molar ratio of GSH/GSSG/peptide was 1:2:1). The solution was stirred slowly for 18 h to allow air oxidation of the peptide before TFA was added at a final concentration of 0.1% to stop the reaction. RP-HPLC, as described above, was used to purify the folded peptide. Fractions with a purity of >95% and the correct mass for the oxidised peptide were pooled, lyophilised and stored at −20 °C.

2.5. NMR spectroscopy

Avt1 samples for NMR experiments were prepared by dissolving the lyophilised peptide to a final peptide concentration of 1.5 mM in 95% H_2O and 5% ^2H_2O, adjusted to pH 5.0. The sample for hydrogen-deuterium exchange experiments, whose pH was pre-adjusted to 5.0 in H_2O, was dissolved in 100% ^2H_2O at a final concentration of 0.5 mM. NMR spectra were acquired on a Bruker Avance III 600 MHz NMR spectrometer equipped with a cryogenically cooled TCI cryoprobe.

One-dimensional (1D) ^1H spectra, two-dimensional (2D) ^1H—^1H total correlation spectroscopy (TOCSY) and 2D ^1H—^1H nuclear Overhauser effect spectroscopy (NOESY) were recorded at 20 °C. TOCSY spectra were acquired with a spin lock time of 100 ms at 20 °C, and NOESY spectra with a 300 ms mixing time. 2D ^1H—^{15}N HSQC (with two different spectral widths, 35 and 50 ppm) and 2D ^1H—^{13}C HSQC spectra were also recorded at 20 °C at ^{15}N and ^{13}C natural abundances. The 2D experiments were acquired with 512 and 2048 complex data points in the t1 and t2 dimensions, respectively, and 64 scans per increment. All NMR data were processed using NMRpipe [51] and analysed using CcpNmr Analysis (version 2.5.2) [52] accessed via the NMRbox platform [53] to obtain a complete assignment of resonances. 1,4 dioxane at 3.75 ppm was used as an internal chemical shift reference in the 1D ^1H dimension, while the ^1H—^{13}C and ^1H—^{15}N spectra were calibrated indirectly [54].

A series of 1D ^1H spectra of Avt1 was recorded over the pH range of

2.0 to 7.0, where the pH of the sample was measured both before and after the acquisition of each spectrum. A further set of 1D ^{1}H NMR spectra was recorded over the temperature range 10–25 °C in increments of 5 °C. Amide proton exchange with deuterium was monitored by acquisition of a series of 1D ^{1}H and 2D TOCSY spectra at 10 °C immediately after dissolving the lyophilised peptide in 100% $^{2}H_2O$.

2.6. Structural restraints and structure calculation

The structure of Avt1 was calculated using distance restraints derived from NOE intensities in 2D ^{1}H—^{1}H NOESY using ARIA version 2.3 [55,56], accessed via NMRbox [53]. Peptide backbone dihedral angles (ϕ and ψ) were calculated from the chemical shifts of the residues using the prediction program TALOS-N [57]. Amino acid residues involved in hydrogen bonds were predicted from both TALOS-N and the hydrogen-deuterium exchange experiments described above. Rapidly exchanging amide protons were not considered to be involved in hydrogen bonds or ordered secondary structure, while slowly exchanging amide protons that were visible in the spectrum 12 h after dissolution were identified as possible hydrogen bond donors in the secondary structure. Initial structures were calculated without defining the disulfide bond restraints in order to determine their connectivity based on the proximities of the Cys SH groups and NOEs between Cys residue sidechains. The three inferred disulfide bonds were used as restraints in the subsequent structure calculations. ARIA generated an ensemble of 100 structures of Avt1, from which the top 20 structures with the lowest energy values were selected for structure analysis using protein structure validation software suite (PSVS) [58]. All structure figures were generated using PyMOL (http://www.pymol.org).

2.7. Electrophysiological assays

2.7.1. Cell cultures and heterologous expression of ion channels

Chinese hamster ovary (CHO) cells (ATCC, Germany) were cultured in DMEM medium (Sigma-Aldrich, St. Louis, MO, USA) supplemented with 10% fetal bovine serum, L-glutamine (2 mM), penicillin-g (100 μg/mL), and streptomycin (100 μg/mL). Cells were maintained in a humidified incubator at 37 °C and 5% CO_2, and passaged twice weekly following a 7 min incubation in 0.05% trypsin–EDTA solution. CHO cells were transiently transfected with plasmids encoding the following ion channels using Lipofectamine 2000 kit (Invitrogen, Waltham, MA, USA) according to the manufacturer's protocol: hK_V1.1 and hK_V1.2 in pCMV6-AC-GFP plasmid, hK_V1.5 in pEYFP-C1 plasmid, hK_{Ca}3.1 in pEGFP-C1 plasmid, hNa_V1.5 in pcDNA 3.1 plasmid and hH_V1 in pQBI25-fC3 plasmid. GFP-positive transfectants were identified using Nikon TE 2000 U fluorescence microscope (Nikon, Tokyo, Japan) and currents were recorded 24 h after transfection. Human embryonic kidney (HEK) 293 cells stably expressing mouse K_{Ca}1.1, hK_V11.1 or hNa_V1.4 channels were used. hTRPV1 channels were expressed in a stable manner in CHO cells. Human K_V1.3 currents were recorded from activated T lymphocytes. For this, mononuclear cells from healthy donors' blood were separated through Histopaque1077 (Sigma-Aldrich, St. Louis, MO, USA) density gradient centrifugation and cultured in RPMI 1640 medium containing 2 mM L-glutamine, 10% fetal bovine serum (FBS), 100 μg/mL streptomycin and 100 U/mL penicillin-g at a density of 5×10^5 cells per mL in a humidified incubator at 37 °C and 5% CO_2. Phytohemagglutinin A was added to the medium at a concentration of 2, 5, 10 μg/mL to enhance the expression of K^+ channels. K_V1.3 currents were recorded after 3–6 days of activation.

2.7.2. Current recording conditions and solutions

Standard whole-cell patch-clamp electrophysiology method was used as described previously [12,39]. All current recordings were made using a Multiclamp 700B or Axopatch 200B amplifier connected to a computer with Axon Digidata1440 or 1550 A digitiser. For data acquisition, Clampex 10.7 software was used (Molecular Devices, Sunnyvale, CA, USA). Micropipettes were pulled from Borosilicate Standard Wall with Filament glass (Harvard Apparatus Co., Holliston, MA, USA) in four stages using a Flaming Brown automatic pipette puller (Sutter Instruments, San Rafael, CA, USA), with a tip resistance of usually 3–6 MΩ in the bath solution. Only those current records were used for data analysis when the leak current at holding potential (V_h) was <10% of peak current at a given test potential.

All the salts and components of the solutions were purchased from Sigma Aldrich, St. Louis, MO, USA. The extracellular (bath) solution (ECS) for recording K_V1.x, K_{Ca} and Na_V currents consisted of (in mM) 145 NaCl, 5 KCl, 2.5 $CaCl_2$, 1 $MgCl_2$, 10 HEPES and 5.5 glucose, pH 7.35. The ECS for K_V11.1 consisted of (in mM) 140 choline-Cl, 5 KCl, 2 $MgCl_2$, 2 $CaCl_2$, 10 HEPES, 20 glucose, 0.1 $CdCl_2$, pH 7.35 and for H_V1 (in mM) 75 NMDG, 3 $MgCl_2$, 1 EGTA, 15 glucose and 180 HEPES, pH 7.4. For the measurement of TRPV1 currents, the ECS and intracellular (pipette) solution (ICS) contained (in mM) 150 NaCl, 2 Na-EDTA and 10 HEPES, pH 7.35. The ICS for K_V1.x or K_{Ca}1.1 consisted of (in mM) 140 KF, 2 $MgCl_2$, 1 $CaCl_2$, 11 EGTA and 10 HEPES pH 7.22. The composition of ICS for Na^+ current recording was (in mM) 10 NaCl, 105 CsF, 10 HEPES, 10 EGTA, pH 7.22; for K_V11.1 (in mM) 140 KCl, 2 $MgCl_2$, 10 HEPES, 10 EGTA, pH 7.3, and for K_{Ca}3.1 (in mM) 150 K-Asp, 5 HEPES, 8.5 $CaCl_2$, 2 $MgCl_2$, 10 EGTA, pH 7.22. ICS for H_V1 constituted of (in mM) 75 NMDG, 3 $MgCl_2$, 1 EGTA, 15 glucose and 180 MES, pH 6.4. The osmolarities of the ECS and ICS were 302–308 mOsM and ~ 295 mOsM, respectively. In the HK-150 and Na^+-free ECS all the Na^+ ions were substituted by K^+ ions or choline-Cl, respectively; other ingredients remained unchanged. In the various TEA^+-containing solutions, Na^+ was substituted by tetraethylammonium-chloride in equimolar concentration. Avt1 peptide and positive controls were dissolved in ECS supplemented with 0.1 mg/mL bovine serum albumin. The measured cell in the recording chamber was perfused with test solutions using a gravity flow micro-perfusion system and AutoMate Perfusion Pencil Multi-Barrel Manifold Tip (AutoMate Scientific, Berkeley, CA, USA), and extra ECS was removed continuously using vacuum suction. The complete exchange of solution in the recording chamber, i.e., the proper operation of the perfusion apparatus, was confirmed frequently using either fully reversible inhibitors (TEA^+ for K_V1.1, K_V1.3 and mK_{Ca}1.1, charybdotoxin (ChTx) for K_V1.2, E4031 for K_V11.1, Cm39 [59] for K_{Ca}3.1 and capsazepine for TRPV1) or ECS (HK-150 solution for K_V1.5, pH 6.4 solution for H_V1 or Na^+ free solution for Na_V channels) as positive controls.

2.7.3. Voltage protocols and data analysis

For recording the currents of K_V1.x channels, 15–300 ms long voltage pulses to +50 mV were applied from a V_h of −120 mV every 15 s and peak currents were measured. For measuring the K_V11.1 currents, a voltage step to +20 mV for 1.25 s from a V_h of −80 mV followed by a step to −40 mV for 2 s was applied every 30 s, and the peak (tail) currents were recorded during the latter step. mK_{Ca}1.1 currents were evoked by depolarizing the cells to +100 mV for 600 ms from a V_h of −100 mV and test pulses were delivered every 15 s. For K_{Ca}3.1 currents, 150-ms-long voltage ramps from −120 mV to +50 mV were applied every 10 s and the V_h was set to −85 mV. For sodium currents through Na_V channels, 15-ms-long voltage steps from a V_h of −120 to 0 mV were applied every 10 s. Currents through H_V1 channel were elicited every 15 s with voltage ramps from −60 mV to +100 mV at a rate of 0.16 mV/ms. TRPV1 currents were elicited every 5 s with 200-ms-long voltage ramps from −50 mV to +50 mV. The cells were held at 0 mV during the subsequent pulses. TRPV1 channels were activated by 1 μM capsaicin prior to the application of capsazepine or Avt1, with the capsaicin-activated current serving as a control.

Patch-clamp records were analysed with pClamp 10.7 software package (Molecular Devices, Sunnyvale, CA, USA). Ionic current traces were digitally filtered with a three-points boxcar smoothing filter and corrected for ohmic leakage when needed. The inhibitory effect of the peptide at a given concentration was calculated as remaining current fraction (RCF = I/I_0, where I_0 is the peak current in the absence of the

toxin, and I is the peak current recorded after 3 min perfusion by 100 nM of Avt1. Representative graphs were prepared using GraphPad Prism software (version 8.0.1, La Jolla, CA, USA).

2.8. Haemolysis assay

To assess potential haemolytic activity of the peptide, a 0.5% suspension of erythrocytes obtained from heparinised peripheral venous blood of a healthy rat was co-incubated with 1 mM Avt1. The erythrocyte suspension was centrifuged using 5 mL heparinised blood for 5 min at 3000 rpm. The plasma and the buffy coat were discarded, and the erythrocytes were washed thrice with PBS at pH 7.2 (Gibco Dulbecco's Phosphate Buffered Saline (1×)). For the negative control, 0.5% (*v*/v) of erythrocyte suspension was prepared using PBS, whereas the positive control was prepared in MilliQ water. The samples were incubated at 37 °C for 30 min with gentle shaking. After incubation, the samples were centrifuged at 3000 rpm for 5 min and the supernatant was separated from the pellet. The absorbance was measured at 540 nm using the Pharmacia type Novaspec II spectrophotometer. Haemolysis was expressed as the following formula:

$$\text{Hemolysis ratio} = (OD_{540}\ (\text{peptide}) - OD_{540}\ (\text{negative control}))\ /(OD_{540}\ (\text{positive control}) - OD_{540}\ (\text{negative control}))\times 100$$

2.9. Proteolysis assays

Proteolysis assays were performed as described previously [34]. The enzymes trypsin (EC 3.4.21.4), α-chymotrypsin (EC 3.4.21.1) and pepsin (EC 3.4.23.1), all with 100 μM concentration stocks, were used in the proteolysis assays at 250:1 peptide/enzyme molar ratio. The reactions for trypsin and α-chymotrypsin were performed in 50 mM Tris-HCl (pH 7.4) buffer containing 100 mM NaCl and 2 mM $CaCl_2$. The reaction for pepsin was performed in 1 mM HCl (pH 2.0). The Avt1 sample was prepared at 25 μM and incubated with enzymes at 37 °C and the reaction was monitored and analysed by LC-MS (0–60% acetonitrile gradient, 10 min) after 0, 0.5, 1, 2, 4 and 16 h of incubation. Trypsin and α-chymotrypsin reactions were halted by adding 1% TFA, and the pepsin reaction was halted by adding 100 mM ammonium bicarbonate (pH 7.4). A cleavable substrate (Ac-SSKSFS) was synthesised in-house and used as a control in the proteolysis assays.

The trypsin inhibitory assay was conducted as described previously [60]. The assay buffer contained 50 mM Tris, 20 mM $CaCl_2$, pH 8.2. 4 mg of bovine pancreatic trypsin was dissolved in 1 mL of 1 mM HCl then diluted into 200 mL of assay buffer and stored on ice. The substrate L-BAPNA (Sigma Aldrich, USA) was prepared in 99% buffer and 1% DMSO at 0.4 mg/mL. Avt1 and the positive control (aprotinin, a bovine pancreatic trypsin inhibitor) were prepared in buffer at 0.3 mM and 0.1 mM concentrations, respectively. To each sample, 5 mL of the substrate solution was added, and samples were incubated at 37 °C for 30 min. 2 mL of trypsin solution then was added to the samples and they were incubated for a further 10 min at 37 °C. The reactions were terminated by adding 1 mL of 30% acetic acid and the absorbances for the sample readings (OD_{410S}) were measured at 410 nm. The reaction was also run in the absence of inhibitors by replacing the sample with water and the corresponding absorbance was the reference reading symbolised as OD_{410R}. In addition, reagent blanks for the sample readings (OD_{410SB}) and reagent blank for the reference reading (OD_{410RB}) were also run by adding the acetic acid solution before the substrate L-BAPNA. All absorbance readings were measured using a Pharmacia Novaspec II spectrophotometer with deionised water as reference. The trypsin inhibitory activity (TIA), which is expressed in trypsin units inhibited (TUI) per mg of sample and % trypsin inhibition were calculated as follows:

$$\text{TIA (TUI/mg)} = [(OD_{410R} - OD_{41RB}) - (OD_{410S} - OD_{41SB})]\ \text{x}\ 100/m_s$$

where, m_s is the mass of the sample in mg per 1 mL of final sample solution.

$$\%\text{trypsin inhibition} = [(OD_{410R} - OD_{41RB}) - (OD_{410S} - OD_{41SB})]/(OD_{410R} - OD_{41RB})\ \text{x}\ 100$$

3. Results

3.1. Identification and amino acid sequence homology of Avt1

The full open-reading frame for Avt1 (MNSKAIISVFLIMLVVVSCTQATYETEDDDEPGPRHSEKR-SCARGCGGDSDCPCPGWHCPSPGGRCEP) was first identified in the transcriptome of *Aulactinia veratra* and the mature peptide sequence (SCARGCGGDSDCPCPGWHCPSPGGRCEP) was identified in the proteome of the secreted venom. Two high quality peptides were found in the MS data which covered 85.7% of the Avt1 sequence, although 100% of the sequence had high confidence (conf ≥95) matches (Table S2). Of the 20 sea anemone transcriptomes analysed (Table S1), eight sequences with similarity to Avt1 were found in five species (Table S3). Each species had two gene copies, except for *Condylactis gigantea*, and sequences were only found in the superfamily Actinioidea. Alignment of the mature peptide sequences revealed strong conservation of three tandem motifs: Asp-Ser between the second and third Cys residues, Pro-Gly-Trp-His between the fourth and fifth Cys, and Gly-Gly between the fifth and sixth Cys (Fig. 1).

3.2. Synthesis and folding of Avt1

The mature Avt1 peptide sequence contains 28 amino acid residues that include six cysteines with a theoretical molecular mass of 2786.04 Da, assuming the formation of three disulfide bonds. Following the solid-phase synthesis of Avt1, the mass of the linear peptide was confirmed using LC-MS (observed mass 2791.58 Da, theoretical mass 2792.09 Da). The crude peptide was purified using RP-HPLC, and fractions were analysed by LC-MS to confirm the identity and purity of the peptide (Fig. S1). Following oxidation of the pure reduced peptide, the folded peptide was re-purified by RP-HPLC and a major peak was eluted with 29% of buffer B (Fig. S2A). LC-MS revealed a pure peak with a molecular mass 6 Da less than the mass of the crude peptide in the reduced form (Fig. S2B), confirming the formation of three disulfide bridges.

3.3. NMR and sequence-specific resonance assignments

The 1D ^{1}H NMR spectrum of Avt1 at pH 5.0 and 20 °C (Fig. 2A) showed that the peaks in the amide/aromatic region are sharp and well-dispersed, indicating that synthetic Avt1 adopts a single major conformation with well-defined tertiary structure (Fig. 2B). Minor peaks visible in the amide and aromatic region may indicate the presence of isomers with *cis* or *trans* conformations about the X–Pro bonds since the sequence contains five prolines; of these, the C-terminal Pro28 is the most likely to have the conformational freedom to enable the co-existence of both isomers.

A series of 1D NMR spectra was then recorded over the pH range 3.0–6.0 (Fig. S3A) to determine the best conditions for resonance assignments and structure calculations. Several backbone amide resonances showed minor changes in chemical shift values as a function of pH, with the best dispersion of the overlapped cross peaks over the amide and aromatic region, specifically between 7.5 and 8 ppm, being observed at pH 5.0 (Fig. S3B). 1D spectra of Avt1 were also recorded at different temperatures from 10 to 25 °C with a 5 °C difference (Fig. S4A and B) at pH 5.0, and the spectrum at 20 °C showed a better peak dispersion through the amide and aromatic region. Therefore, all spectra used for sequential assignments were recorded at pH 5.0 and 20 °C.

Sequential backbone and sidechain chemical shift assignments were

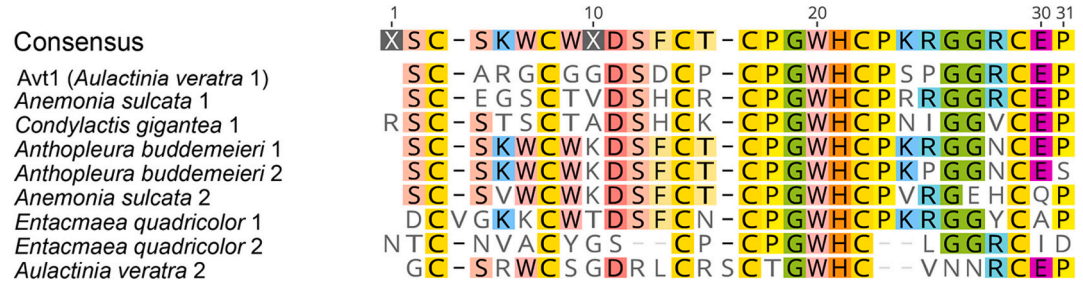

Fig. 1. Alignment of the mature peptide sequences for Avt1 and eight homologous sequences found in sea anemones. The consensus sequence represents the dominant amino acid residue for each position in the sequence. NCBI accession numbers are SRX971488, PRJEB21970, PRJNA313244, PRJNA313244, SRX971488, PRJEB21970, PRJEB21970 and PRJNA313244, respectively (Table S1).

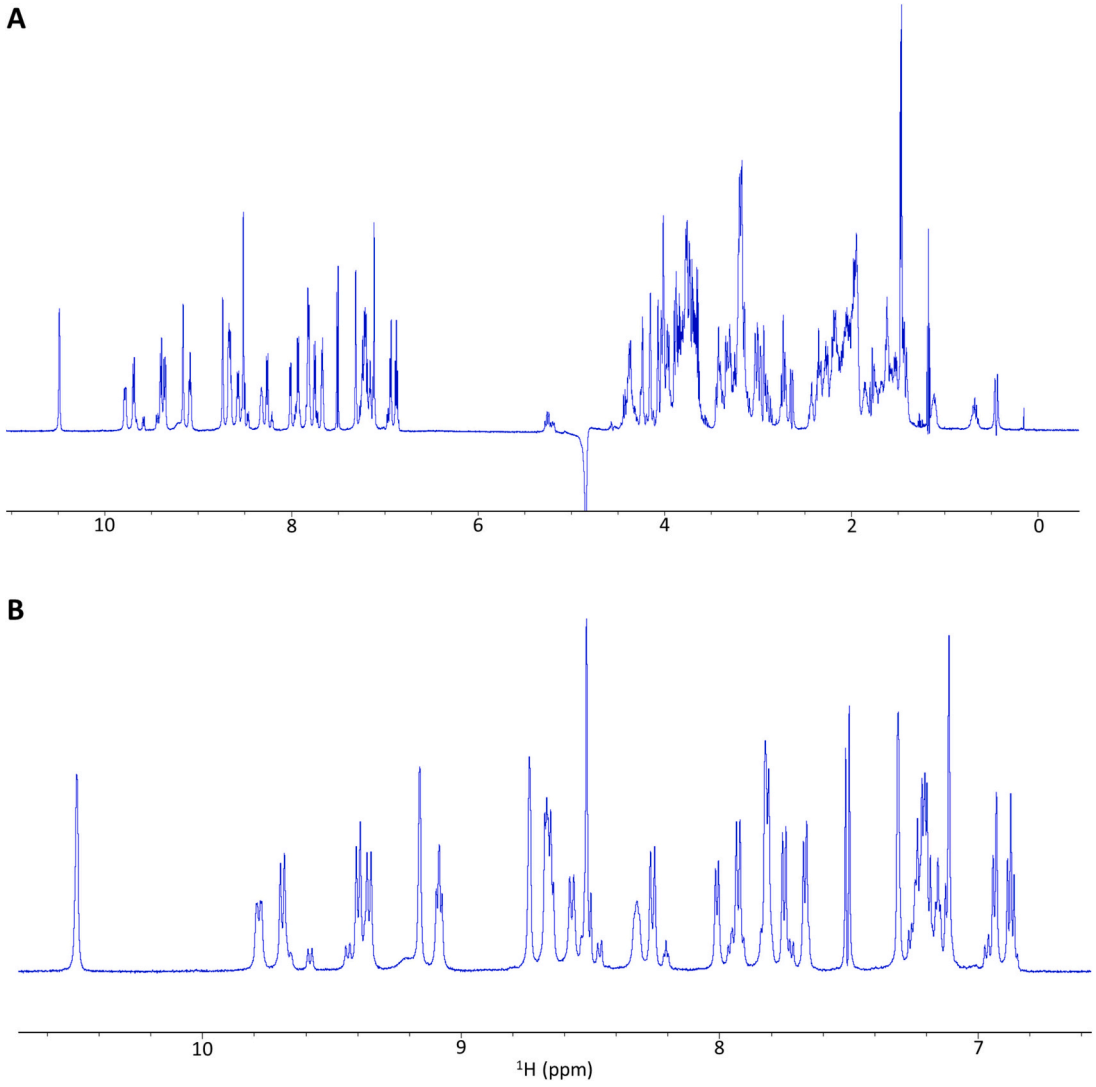

Fig. 2. 1D ^{1}H NMR spectrum of Avt1 in 95% H_2O and 5% ^2H_2O, acquired on a Bruker 600 MHz NMR spectrometer at pH 5.0 and 20 °C. A. Full spectrum of Avt1. B. Expanded amide and aromatic region.

completed by analysis of 2D [^{1}H–^{1}H] TOCSY, 2D [^{1}H–^{1}H] NOESY, 2D [^{1}H–^{15}N] HSQC and 2D [^{1}H–^{13}C] HSQC spectra. Fig. 3 shows the 2D [^{1}H–^{15}N] HSQC spectrum with the assignment of the backbone cross peaks of the residues except for the N-terminal Ser1 and proline residues (Pro13, Pro15, Pro20, Pro22 and Pro28). Two different spectral widths in the ^{15}N dimension were used (35 ppm in green and 50 ppm in blue) as Arg4 and Arg25 side chain folded peaks were identified with the increased ^{15}N spectral width. Fig. S5 shows an assigned and labelled 2D [^{1}H–^{13}C] HSQC spectrum. Table S4 summarises the ^{1}H, ^{15}N and ^{13}C chemical shifts of Avt1. The chemical shift were deposited in the BioMagResBank with accession number 52543 [61].

3.4. Disulfide determination and structure calculation

The solution structure of synthetic Avt1 was calculated using a total of 801 NOE-derived distance restraints as follows: 358 are intra-residue,

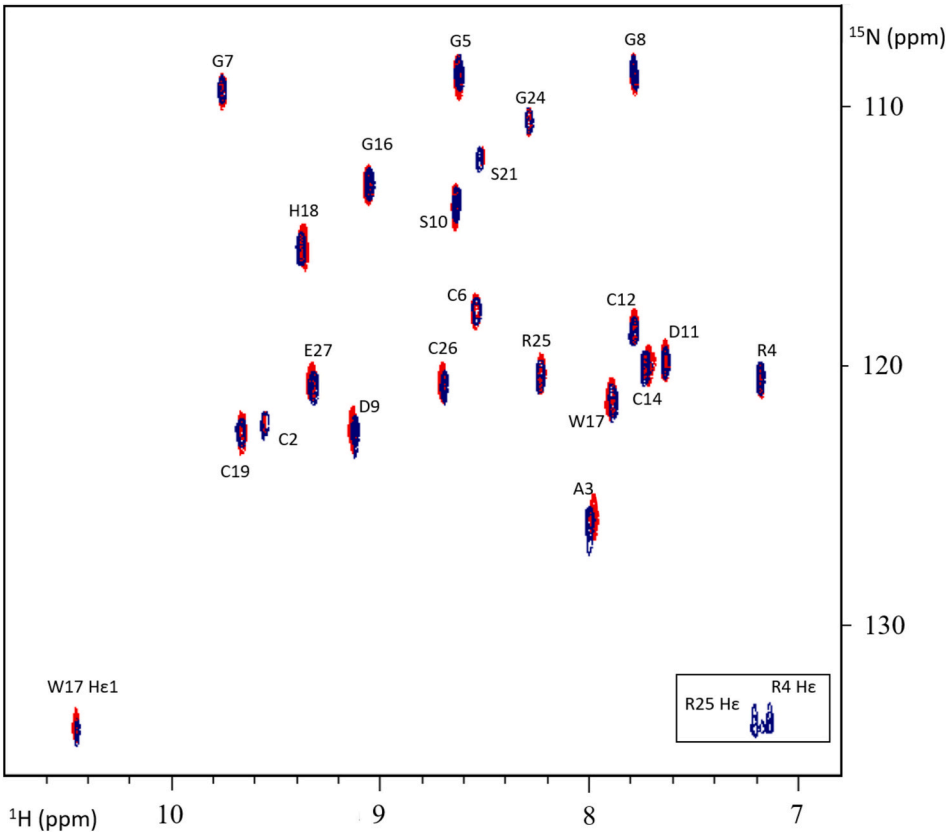

Fig. 3. 2D [^{1}H–^{15}N] HSQC spectra of Avt1 with resonance assignments. The spectra were acquired on a Bruker 600 MHz NMR spectrometer at pH 5.0 and 20 °C. Two different spectral width in ^{15}N dimension were used: 35 ppm in red and 50 ppm in blue. Folded peaks are boxed. (For interpretation of the references to colour in this figure legend, the reader is referred to the web version of this article.)

183 sequential, 92 medium-range ($2 \leq |i-j| \leq 5$) and 168 long-range ($|i-j| > 5$) restraints (Table 1). Twelve dihedral restraints as well as eight hydrogen bond restraints derived from hydrogen-deuterium exchange experiments (Fig. S6) and TALOS-N prediction [57] were included. Altogether, the final experimental set corresponded to an average of 28 restraints per residue.

The initial structures were calculated based on NOE restraints without specifying the disulfide connectivity. Following the convergence of the initial structures, the disulfide bond connectivities were well-defined based on the proximity of the cysteine residues and the NOEs of the sidechains, and were included in the subsequent runs. Accordingly, the disulfide linkage was determined as I-IV, II-V and III-VI which is found in inhibitory peptides from diverse biological sources [62,63]. Fig. 4A shows a stereo view of the final ensemble of 20 lowest energy structures that were energetically refined through MD simulation in explicit water using ARIA. The structures are well-defined, with backbone (N, C and Cα) and all heavy atom root mean square deviation (RMSD) values over all residues of 0.5 and 0.9 Å, respectively. Table 1 summarises the structural statistics.

Table 1.
List of restraints and statistical analysis of Avt1 structure at pH 5.0 and 20 °C.

Number of experimental restraints	
Total NOE distance restraints	801
Intra-residue	358
Inter-residue	
Sequential	183
Medium range ($2 \leq \|i-j\| \leq 5$)	92
Long range ($\|i-j\| > 5$)	168
Torsion angle (phi/psi)	12
H-bond restraints	8
RMSD from average structure	
All backbone atoms, all residues (N, Cα, C) (Å)	0.5
All heavy atoms, all residues (Å)	0.9
RMS deviation for bond angles (°)	0.6
RMS deviation for bond lengths (Å)	0.004
Ramachandran statistics (Molprobity) of ordered residue	
Most favoured regions (%)	85.00
Additionally allowed regions (%)	14.10
Generously allowed regions (%)	0.30
Disallowed regions (%)	0.60
Ramachandran statistics (Procheck) of ordered residues	
Most favoured regions (%)	93.70
Allowed regions (%)	5.20
Disallowed regions (%)	1.20

Avt1 has a well-defined core structure stabilised by three disulfide bonds adopting an inhibitor cystine knot (ICK) motif in which two disulfide Cys2- Cys14 and Cys6- Cys19 form a closed ring with a third disulfide Cys19- Cys26 penetrating the ring to create the pseudo-knot [63]. Four loops emerge from this compact disulfide core (Ala3-Gly5, Gly7-Asp11, Pro15-His18 and Pro20-Arg25), in addition to N and C termini (Fig. 4B). The β-sheet motif typically present in peptides adopting an ICK scaffold was not observed in Avt1. The flexible N-terminus adopts an extended conformation up to residue seven followed by a short turn of 3_{10} helix spanning residues Asp9-Asp11. The five proline residues (Pro13, Pro15, Pro20, Pro22 and Pro28) were observed in the *trans* conformation and assigned clearly by the strong sequential $d_{\alpha\delta}$ NOEs between the proline residues and their preceding α-protons (Fig. S7). Furthermore, the 2D [^{1}H–^{13}C] HSQC spectrum showed that the chemical shift difference between Cβ and Cγ of Pro15, Pro20 and Pro22 was less than 5 ppm, supporting the *trans* geometry of those proline peptide bonds [64]. Avt1 has three positive residues (Arg4, His18 and Arg25) and three negative residues (Asp9, Asp11 and Glu27) that are evenly distributed throughout the peptide surface (Fig. 5). Like other

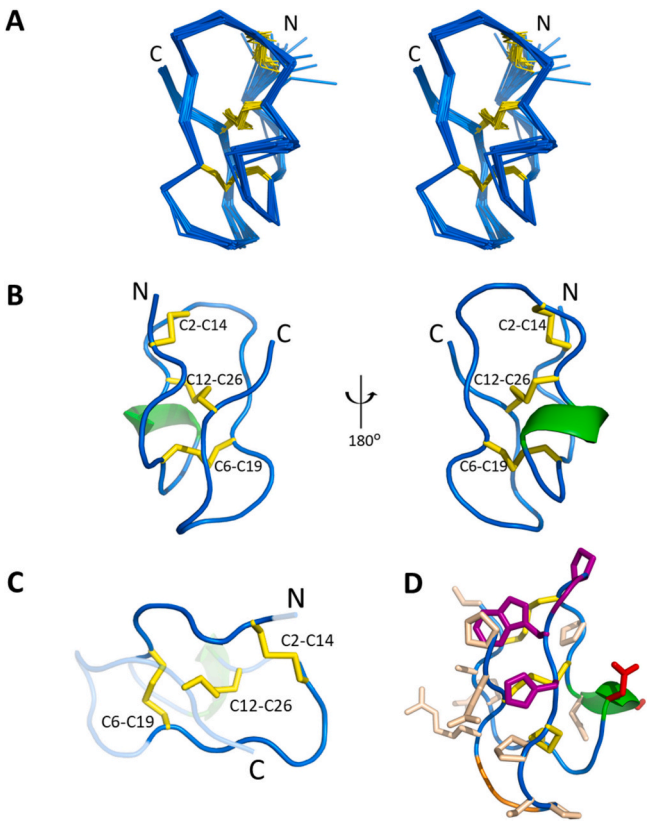

Fig. 4. Avt1 solution structure. A. Stereo view (cross-eyed) of the structure of Avt1. The top 20 structures of Avt1 with lowest energy overlaid for the best fit over the backbone heavy atoms of residues 1–28, represented as ribbon in blue and the three disulfide bonds in yellow. B. Cartoon representation of the lowest energy Avt1 structure. The single turn of 3_{10}-helix is coloured green. N and C are labelled and the position of Cys residues are indicated as C2-C14, C6-C19 and C12-C26. C. The cystine knot of Avt1 comprises a ring formed by two disulfide bonds (C2-C14 and C6-C19) with a third disulfide bond (C12-C26) penetrating the ring to create a pseudo-knot. D. The lowest energy structure of Avt1 showing all side chains, with the disulfides in yellow, Pro-Gly-Trp-His in purple, Asp-Ser in red and Gly-Gly in orange. (For interpretation of the references to colour in this figure legend, the reader is referred to the web version of this article.)

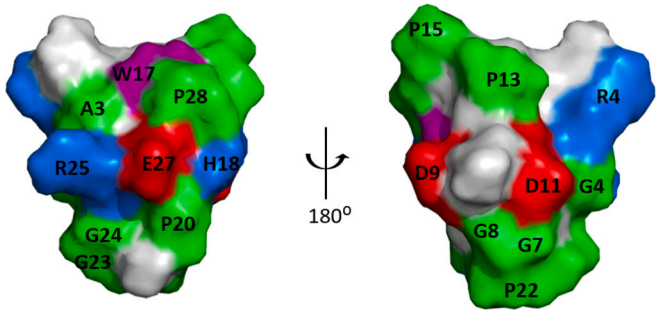

Fig. 5. Surface representation of Avt1 showing the negatively charged side chains (Asp9, Asp11 and Glu27) in red, the positively charged (Arg4, His18 and Arg25) in blue, the hydrophobic residue (Trp17) in magenta, non-polar residues in green and all others in grey. (For interpretation of the references to colour in this figure legend, the reader is referred to the web version of this article.)

disulfide-rich peptides, Avt1 lacks the classical hydrophobic core found in structured peptides and proteins as the disulfide bonds themselves comprise the core [65]. The sidechain of Trp17 is largely solvent exposed and cannot be considered as a part of the hydrophobic core, while Ala3 is partially buried.

A search using RCSB PDB [66] identified the ICK toxins Magi 5, ω-conotoxin GVIA and EETI-II (Fig. 6) as the closest structural homologues. Magi 5 (PDB id 2GX1), a 29-residue peptide from the hexathelid spider *Macrothele gigas*, targets voltage-gated sodium channels [67]. ω-Conotoxin GVIA (PDB id 1TTL), a 27-residue peptide isolated from the venom of the cone shell *Conus geographus*, is a N-type calcium channel inhibitor [68]. EETI-II (PDB id 2IT7), a 28-residue peptide isolated from seeds of the jumping cucumber *Ecballium elaterium*, is a potent trypsin inhibitor [69]. While these four structures are similar, with all of them having an ICK fold, it is evident from Fig. 6 that they have distinct secondary structures.

It is of interest to compare the solution structure determined in this study with that predicted by AlphaFold2 [70]. The top-scoring predicted structure matched the experimental structure quite well (RMSD over backbone heavy atoms of 0.82 Å), but other predicted structures that lacked one of the three native disulfide bridges had confidence scores that were not significantly worse than the correct structure, implying that experimental structure determination was warranted.

3.5. Ion channel activity

To identify potential targets of this peptide, Avt1 was tested against a wide range of mammalian ion channels using electrophysiological assays. The whole-cell currents were recorded under controlled conditions and then the micro-perfusion system functionality was confirmed using reversible blockers of the respective channels. After confirming proper solution exchange, cells were perfused with Avt1 and the whole-cell currents were recorded (Fig. 7A-K). The peptide was investigated on human voltage-gated potassium channels ($K_V1.1$, $K_V1.2$, $K_V1.3$, $K_V1.5$ and $K_V11.1$) expressed in various expression systems (see Materials and Methods). None of the different K_V channel isoforms was inhibited by 100 nM Avt1. The peptide was also tested against two human voltage-gated sodium channels ($Na_V1.4$ and $Na_V1.5$) and no inhibition was detected by 100 nM Avt1. The screening was then expanded to study

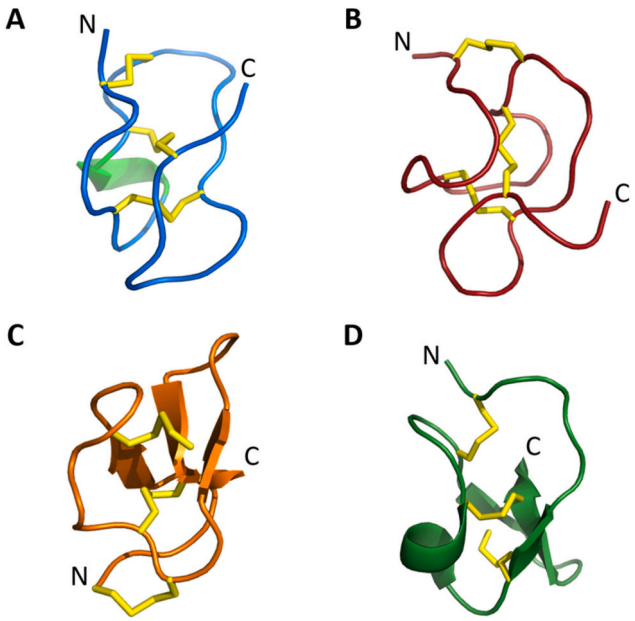

Fig. 6. Structural homologues of Avt1 peptide. A. Avt1 in blue. B. Magi 5 in red (PDB id 2GX1) isolated from the hexathelid spider *Macrothele gigas*. C. ω-Conotoxin GIVA in orange (PDB id 1TTL) from the cone shell *Conus geographus*. D. Squash trypsin inhibitor EETI-II (PDB id 2IT7) isolated from seeds of the jumping cucumber *Ecballium elaterium*. (For interpretation of the references to colour in this figure legend, the reader is referred to the web version of this article.)

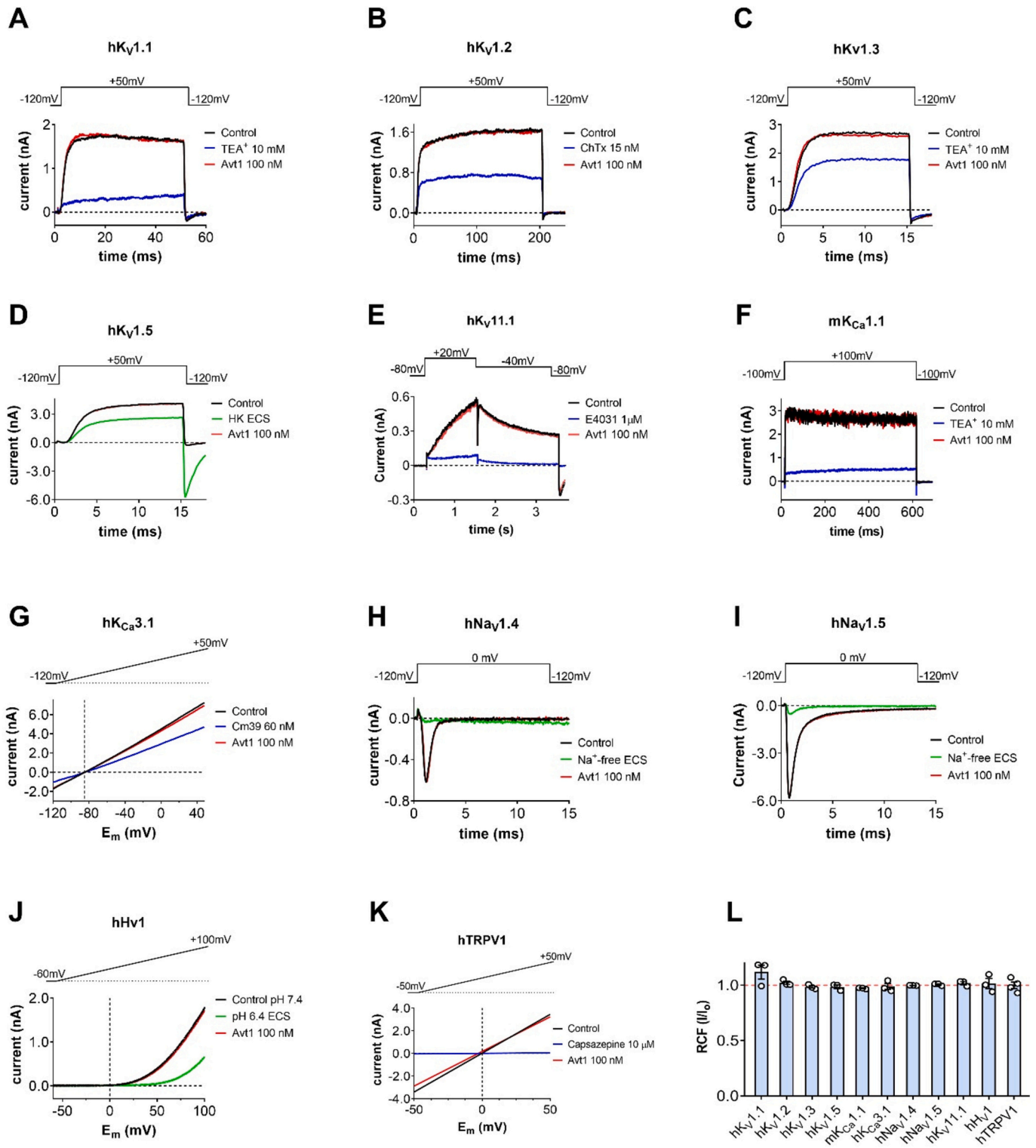

Fig. 7. Avt1 is ineffective against several mammalian ion channels including K^+, Na^+, H^+ and TRP channels. A-K. Representative current traces of various ion channels recorded before application of Avt1 (control, black traces) and after 3 min perfusion with 100 nM of Avt1 (red traces). The complete solution exchange in the recording chamber was confirmed before each experiment with specific inhibitors of the respective channel (blue traces, TEA^+: tetraethylammonium chloride; ChTx: charybdotoxin; E4031; Cm39 toxin; capsazepine) or ECS solutions as control (green traces, HK: HK-150 solution with 150 mM extracellular K^+; Na^+-free ECS solution: Na^+ substituted by choline-Cl; pH 6.4 ECS: ECS with pH 6.4 for hH_V1). The horizonal dashed line shows the zero-current level. Voltage protocols are shown above the current traces in each panel. For details on the expression systems, external and internal solutions, and voltage protocols, see the Materials and methods. For $hK_{Ca}3.1$, hH_V1 and hTRPV1, the currents were evoked in response to a voltage ramp, corrected for ohmic leakage and showed as a function of test potential (E_m). The vertical dashed line in panels G and K indicate the expected reversal potential of the currents based on the Nernst eq. L. Bar graph represents the summary of Avt1 effect at 100 nM; error bars represent SEM, circles indicate individual data points, $n = 3$–4. (For interpretation of the references to colour in this figure legend, the reader is referred to the web version of this article.)

other ion channels including $mK_{Ca}1.1$, $hK_{Ca}3.1$, hTRPV1 and hH_V1, but none was inhibited significantly by Avt1 at 100 nM (Fig. 7L).

3.6. Haemolytic assay

Several toxins adopting cystine knot structures exhibit haemolytic activity [71,72]. Therefore, the haemolytic effect of Avt1 was investigated in healthy rat erythrocytes, but the peptide showed no haemolytic activity when tested at 1 mM (Fig. S8). This could be due to the lack of a significant solvent-exposed hydrophobic patch that is commonly found in haemolytic peptides such as kalata B1 (PDB id 1NB1) and others, as this feature is proposed to be important for peptide binding to the erythrocyte membrane [71].

3.7. Proteolysis assays

The stability of Avt1 peptide was tested upon treatment with the proteases trypsin, chymotrypsin and pepsin. Avt1 showed high stability in the presence of trypsin or chymotrypsin over 16 h of incubation at 37 °C (Fig. S9A and B). The peptide was not cleaved by trypsin, which cleaves peptide bonds at the C-terminus of Arg and Lys residues, or chymotrypsin, which cleaves the C-terminal side of aromatic and hydrophobic residues, despite the presence of cleavable sites in Avt1 such as Arg and Trp, consistent with the fact that these sites are partially buried in the structure. In the presence of pepsin, which cleaves peptide bonds N-terminal to aromatic residues, Avt1 was not affected over 16 h of incubation at 37 °C (Fig. S9C), despite the presence of Trp as a potential cleavage site. The activity of the enzymes was confirmed using a small cleavable substrate containing Lys and Phe as a control.

The trypsin inhibitory activity of Avt1 then was assessed because of its structural homology to the trypsin inhibitory peptide EETI-II (PDB id 2IT7), as documented above. Avt1 did not inhibit trypsin when tested at 0.3 mM and obtained a low TIA value of 0.5 TIU/mg when compared to the TIA value of the bovine pancreatic trypsin inhibitor Aprotinin, 106 TUI/mg. The trypsin inhibition activities of Avt1 and Aprotinin were 0.75 and 99.90%, respectively (Fig. S10).

4. Discussion

Transcriptomic and proteomic data showed the presence of the Avt1 peptide in milked venom of the sea anemone *Aulactinia veratra*, and homologues of this peptide are found in sea anemone species from superfamily Actinioideae. Multiple copies of the gene encoding this peptide were found in these species, indicating that it has undergone a gene duplication event like several other sea anemone peptide toxins [73–75]. Avt1 was synthesised and folded using an *in vitro* oxidative folding method, and its solution structure was determined using NMR spectroscopy.

Avt1 adopts an ICK fold, which is one of the most widespread convergently recruited disulfide-rich peptide scaffolds in venomous animals, such as scorpions, spiders and cone snails [76,77]. The disulfide connectivity in an ICK motif has a C1-C4, C2-C5 and C3-C6 pattern, which provides a compact and highly stable scaffold [78,79]. The major conformations of the peptide bonds preceding all five proline residues in Avt1 were found to be *trans*. The minor peaks visible in the amide and aromatic region of the 1D ^{1}H NMR spectrum may be due to the presence of the *cis* isomer of one of these proline residues. As the least structurally constrained proline is the C-terminal Pro28, we anticipate that the minor conformer may be the *cis* conformer of the peptide bond preceding this proline.

Proteolytic stability is an important consideration in the development of peptides as molecular tools, therapeutic leads or bioinsecticides. For peptides that function in venoms, proteolytic stability is believed to contribute to their ability to function in hostile environments (such as the circulation systems of prey organisms). Avt1 was resistant to three proteases despite the presence of multiple potential cleavage sites in the peptide sequence (Arg4, Arg25 and Trp17). These cleavage sites are presumably protected from proteases binding by the compact folding of the cystine knot. Similar high proteolytic stability was reported for ProTx-II (PDB id 2N9T), a spider ICK toxin that also lacks the typical β-sheet motif [80], despite the presence of several potential digestion sites in the sequence. The removal of one disulfide linkage in another ICK peptide appeared to compromise the resistance of these peptides to proteolysis without affecting the three-dimensional structure [81]; it seems that the remarkable resistance of ICK peptides to proteolysis is mainly a consequence of the disulfide-stabilised structure rather than their amino acid sequence or even cyclisation [82]. The resistance to proteolysis is consistent with a role for Avt1 in defence and/or the capture of prey by *Aulactinia veratra*, but our functional studies have not yet identified what that role might be.

The Avt1 structure is the first representative of a new family of sea anemone peptides to be characterised structurally and functionally. As shown in Fig. 1, this family has strong conservation of three tandem motifs: Asp-Ser between the second and third Cys residues, Pro-Gly-Trp-His between the fourth and fifth Cys, and Gly-Gly between the fifth and sixth Cys. Based on the locations of these sequences in the structure (Fig. 4D), it is likely that the conserved Asp-Ser sequence (in red) may have a functional role given that these two side chains are solvent-exposed, the conserved Pro-Gly-Trp sequence (in purple) probably has a structural role, although the conserved His (also in purple) may have a functional role, while the conserved Gly-Gly sequence (in orange) is most likely to have a structural role.

Although Avt1 was found in the milked venom of *Aulactinia veratra*, it was not active against several mammalian ion channels in electrophysiological assays. Structurally, Avt1 is closely related to the sodium channel toxin Magi 5 from the spider *Macrothele gigas* [67], which has been found to bind specifically to receptor site 4 in mammalian Na_V channels and compete with scorpion β-toxins, such as Css4 from *Centruroides suffusus suffusus* [67,83]. Magi 5 has an interactive surface that is highly charged on one side, with five Lys residues, and hydrophobic residues on the other, as well as a negatively charged residue (Glu) involved in voltage sensor trapping [67]. These characteristics are widely described as important for interaction with receptor site 4 on mammalian Na_V channels [84,85]. Although Avt1 contains positively charged residues and one Glu, it was not active against several subtypes of the mammalian Na_V channels. It is well established that highly positively charged surfaces are crucial for binding to several mammalian ion channels, as seen in many toxins including ICK toxins [67,86,87]. The less cationic nature of Avt1, with only three positive residues (Arg4, His18 and Arg25) (Fig. 5), may be at least partially responsible for the lack of activity against mammalian sodium channels.

In the Avt1 structure, Glu27 is surrounded by a hydrophobic residue (Trp17) and a non-polar region (Ala3, Pro20, Gly24, Pro28), adjacent to positively charged amino acids (His18, Arg25) forming a patch at the C-terminus (Fig. 5). A similar spatial arrangement with at least one hydrophobic residue in a non-polar region is found in scorpion β-toxins that specifically target insect sodium channels, such as Bj-xtrIT from *Hottentotta judaicus* and AahIT from *Androctonus australis hector* [88,89]. A comparison of Bj-xtrIT structure with other scorpion β-toxins that are active on mammals, showed that this functional cluster at the C-terminus is conserved among toxins specifically targeting insects [90]. This suggest that Avt1 might exhibit an effect against insect sodium ion channels.

In conclusion, Avt1 was identified from transcriptomic and proteomic studies of *Aulactinia veratra*. The solution structure of Avt1 was determined to adopt an ICK fold, which is very similar to several peptide toxins from venomous animals that target ion channels. While Avt1 was not active against a range of mammalian ion channels, including K_V and Na_V channels, it possessed structural features similar to toxins specifically targeting Na_V channels in insects.

Accession codes

The NMR chemical shifts have been deposited in BioMagResBank with id 52543 and the solution structure has been deposited in the Protein Data Bank with PDB id 9CRB

CRediT authorship contribution statement

Renad A. Albar: Writing – review & editing, Writing – original draft, Visualization, Methodology, Investigation, Formal analysis, Data curation. **Hayden L. Smith:** Writing – review & editing, Investigation, Formal analysis, Data curation. **Karoline Sanches:** Writing – review & editing, Methodology, Formal analysis, Data curation. **Dorothy C.C. Wai:** Writing – review & editing, Supervision. **Muhammad Umair Naseem:** Writing – review & editing, Methodology, Investigation, Formal analysis, Data curation. **Tibor G. Szanto:** Writing – review & editing, Visualization, Methodology, Investigation, Formal analysis, Data curation. **Gyorgy Panyi:** Writing – review & editing, Supervision, Formal analysis, Data curation. **Peter J. Prentis:** Writing – review & editing, Supervision, Data curation. **Raymond S. Norton:** Writing – review & editing, Visualization, Supervision, Conceptualization.

Declaration of competing interest

The authors declare that they have no competing financial interests or personal relationships that could have appeared to influence the results reported in this paper.

Data availability

The NMR chemical shifts have been deposited in BioMagResBank with id 52543 and the solution structure has been deposited in the Protein Data Bank with PDB id 9CRB. Other data will be made available on request.

Acknowledgements

RAA acknowledges support from the Saudi Arabian Cultural Mission in Australia and Prince Sattam bin Abdulaziz University (Saudi Arabia). This work was funded in part by the Hungarian National Research, Development and Innovation Office (K143071 to GP) and by a Stipendium Hungaricum Scholarship from the Tempus Public Foundation (to MUN).

Appendix A. Supplementary data

Supplementary data to this article can be found online at https://doi.org/10.1016/j.bbapap.2024.141050.

References

[1] C. Menezes, N.L. Thakur, Sea anemone venom: ecological interactions and bioactive potential, Toxicon 208 (2022) 31–46.
[2] M. Jouiaei, A.A. Yanagihara, B. Madio, T.J. Nevalainen, P.F. Alewood, B.G. Fry, Ancient venom systems: a review on Cnidaria toxins, Toxins (Basel) 7 (2015) 2251–2271.
[3] B. Madio, E.A.B. Undheim, G.F. King, Revisiting venom of the sea anemone *Stichodactyla haddoni*: omics techniques reveal the complete toxin arsenal of a well-studied sea anemone genus, J. Proteome 166 (2017) 83–92.
[4] L. Béress, Biologically active compounds from coelenterates, Pure Appl. Chem. 54 (1982) 1981–1994.
[5] T. Honma, K. Shiomi, Peptide toxins in sea anemones: structural and functional aspects, Mar. Biotechnol. (N.Y.) 8 (2006) 1–10.
[6] R.S. Norton, Structures of sea anemone toxins, Toxicon 54 (2009) 1075–1088.
[7] P.J. Prentis, A. Pavasovic, R.S. Norton, Sea anemones: quiet achievers in the field of peptide toxins, Toxins (Basel) 10 (2018).
[8] J. Fu, Y. Liao, A.H. Jin, B. Gao, Discovery of novel peptide neurotoxins from sea anemone species, Front. Biosci. 26 (2021) 1256–1273.
[9] R.S. Norton, Structure and structure-function relationships of sea anemone proteins that interact with the sodium channel, Toxicon 29 (1991) 1051–1084.
[10] O. Castañeda, V. Sotolongo, A.M. Amor, R. Stocklin, A.J. Anderson, A.L. Harvey, A. Engstrom, C. Wernstedt, E. Karlsson, Characterization of a potassium channel toxin from the Caribbean Sea anemone *Stichodactyla helianthus*, Toxicon 33 (1995) 603–613.
[11] I. Gladkikh, S. Peigneur, O. Sintsova, E. Lopes Pinheiro-Junior, A. Klimovich, A. Menshov, A. Kalinovsky, M. Isaeva, M. Monastyrnaya, E. Kozlovskaya, J. Tytgat, E. Leychenko, Kunitz-type peptides from the sea anemone *Heteractis crispa* demonstrate potassium channel blocking and anti-inflammatory activities, Biomedicines 8 (2020) 473.
[12] K.A. Elnahriry, D.C.C. Wai, L.M. Ashwood, M.U. Naseem, T.G. Szanto, S. Guo, G. Panyi, P.J. Prentis, R.S. Norton, Structural and functional characterisation of Tst2, a novel TRPV1 inhibitory peptide from the Australian sea anemone *Telmatactis stephensoni*, Biochim. Biophys. Acta, Proteins Proteomics 1872 (2024) 140952.
[13] E.N. Grafskaia, N.F. Polina, V.V. Babenko, D.D. Kharlampieva, P.A. Bobrovsky, V. A. Manuvera, T.E. Farafonova, N.A. Anikanov, V.N. Lazarev, Discovery of novel antimicrobial peptides: a transcriptomic study of the sea anemone *Cnidopus japonicus*, J. Bioinforma. Comput. Biol. 16 (2018) 1840006.
[14] Y.A. Logashina, R.G. Solstad, K.S. Mineev, Y.V. Korolkova, I.V. Mosharova, I. A. Dyachenko, V.A. Palikov, Y.A. Palikova, A.N. Murashev, A.S. Arseniev, S. A. Kozlov, K. Stensvag, T. Haug, Y.A. Andreev, New disulfide-stabilized fold provides sea anemone peptide to exhibit both antimicrobial and TRPA1 potentiating properties, Toxins (Basel) 9 (2017) 154.
[15] F. Bosmans, J. Tytgat, Sea anemone venom as a source of insecticidal peptides acting on voltage-gated Na^+ channels, Toxicon 49 (2007) 550–560.
[16] M. Gur Barzilai, R. Kahn, N. Regev, D. Gordon, Y. Moran, M. Gurevitz, The specificity of Av3 sea anemone toxin for arthropods is determined at linker DI/SS2-S6 in the pore module of target sodium channels, Biochem. J. 463 (2014) 271–277.
[17] C.H. Kim, Y.J. Lee, H.J. Go, H.Y. Oh, T.K. Lee, J.B. Park, N.G. Park, Defensin-neurotoxin dyad in a basally branching metazoan sea anemone, FEBS J. 284 (2017) 3320–3338.
[18] P. Lagos, R. Duran, C. Cervenansky, J.C. Freitas, R. Silveira, Identification of hemolytic and neuroactive fractions in the venom of the sea anemone *Bunodosoma cangicum*, Braz. J. Med. Biol. Res. 34 (2001) 895–902.
[19] J.G. McGivern, Ziconotide: a review of its pharmacology and use in the treatment of pain, Neuropsychiatr. Dis. Treat. 3 (2007) 69–85.
[20] G.F. King, Venoms as a platform for human drugs: translating toxins into therapeutics, Expert. Opin. Biol. Ther. 11 (2011) 1469–1484.
[21] S. Bhavsar, S. Mudaliar, A. Cherrington, Evolution of exenatide as a diabetes therapeutic, Curr. Diabetes Rev. 9 (2013) 161–193.
[22] M.W. Pennington, A. Czerwinski, R.S. Norton, Peptide therapeutics from venom: current status and potential, Bioorg. Med. Chem. 26 (2018) 2738–2758.
[23] M. Muttenthaler, G.F. King, D.J. Adams, P.F. Alewood, Trends in peptide drug discovery, Nat. Rev. Drug Discov. 20 (2021) 309–325.
[24] M.W. Pennington, C. Beeton, C.A. Galea, B.J. Smith, V. Chi, K.P. Monaghan, A. Garcia, S. Rangaraju, A. Giuffrida, D. Plank, G. Crossley, D. Nugent, I. Khaytin, Y. Lefievre, I. Peshenko, C. Dixon, S. Chauhan, A. Orzel, T. Inoue, X. Hu, R. V. Moore, R.S. Norton, K.G. Chandy, Engineering a stable and selective peptide blocker of the Kv1.3 channel in T lymphocytes, Mol. Pharmacol. 75 (2009) 762–773.
[25] J.E. Tudor, P.K. Pallaghy, M.W. Pennington, R.S. Norton, Solution structure of ShK toxin, a novel potassium channel inhibitor from a sea anemone, Nat. Struct. Biol. 3 (1996) 317–320.
[26] E.J. Tarcha, C.M. Olsen, P. Probst, D. Peckham, E.J. Munoz-Elias, J.G. Kruger, S. P. Iadonato, Safety and pharmacodynamics of dalazatide, a Kv1.3 channel inhibitor, in the treatment of plaque psoriasis: a randomized phase 1b trial, PLoS ONE 12 (2017) e0180762.
[27] D. Dominguez-Perez, A. Campos, A. Alexei Rodriguez, M.V. Turkina, T. Ribeiro, H. Osorio, V. Vasconcelos, A. Antunes, Proteomic analyses of the unexplored sea anemone *Bunodactis verrucosa*, Mar. Drugs 16 (2018) 42.
[28] O. Sintsova, I. Gladkikh, V. Chausova, M. Monastyrnaya, S. Anastyuk, O. Chernikov, E. Yurchenko, D. Aminin, M. Isaeva, E. Leychenko, E. Kozlovskaya, Peptide fingerprinting of the sea anemone *Heteractis magnifica* mucus revealed neurotoxins, Kunitz-type proteinase inhibitors and a new β-defensin α-amylase inhibitor, J. Proteome 173 (2018) 12–21.
[29] A. Delgado, C. Benedict, J. Macrander, M. Daly, Ever Make Never, an Enemy..., Out of an anemone: transcriptomic comparison of clownfish hosting sea anemone venoms, Mar. Drugs 20 (2022) 730.
[30] M.L. Mitchell, G.Q. Tonkin-Hill, R.A.V. Morales, A.W. Purcell, A.T. Papenfuss, R. S. Norton, Tentacle transcriptomes of the speckled anemone (Actiniaria: Actiniidae: Oulactis sp.): venom-related components and their domain structure, Mar. Biotechnol. (N.Y.) 22 (2020) 207–219.
[31] L.M. Ashwood, K.A. Elnahriry, Z.K. Stewart, T. Shafee, M.U. Naseem, T.G. Szanto, C.A. van der Burg, H.L. Smith, J.M. Surm, E.A.B. Undheim, B. Madio, B. R. Hamilton, S. Guo, D.C.C. Wai, V.L. Coyne, M.J. Phillips, K.J. Dudley, D. A. Hurwood, G. Panyi, G.F. King, A. Pavasovic, R.S. Norton, P.J. Prentis, Genomic, functional and structural analyses elucidate evolutionary innovation within the sea anemone 8 toxin family, BMC Biol. 21 (2023) 121.
[32] M.E. Mazzi Esquinca, C.N. Correa, G. Marques de Barros, H. Montenegro, L. Mantovani de Castro, Multiomic approach for bioprospection: investigation of toxins and peptides of Brazilian sea anemone *Bunodosoma caissarum*, Mar. Drugs 21 (2023) 197.
[33] Q. Guo, J. Fu, L. Yuan, Y. Liao, M. Li, X. Li, B. Yi, J. Zhang, B. Gao, Diversity analysis of sea anemone peptide toxins in different tissues of *Heteractis crispa* based on transcriptomics, Sci. Rep. 14 (2024) 7684.

[34] B. Krishnarjuna, C.A. MacRaild, P. Sunanda, R.A.V. Morales, S. Peigneur, J. Macrander, H.H. Yu, M. Daly, S. Raghothama, V. Dhawan, S. Chauhan, J. Tytgat, M.W. Pennington, R.S. Norton, Structure, folding and stability of a minimal homologue from *Anemonia sulcata* of the sea anemone potassium channel blocker ShK, Peptides 99 (2018) 169–178.

[35] B. Krishnarjuna, J. Villegas-Moreno, M.L. Mitchell, A. Csoti, S. Peigneur, C. Amero, M.W. Pennington, J. Tytgat, G. Panyi, R.S. Norton, Synthesis, folding, structure and activity of a predicted peptide from the sea anemone *Oulactis* sp. with an ShKT fold, Toxicon 150 (2018) 50–59.

[36] P. Sunanda, B. Krishnarjuna, S. Peigneur, M.L. Mitchell, R. Estrada, J. Villegas-Moreno, M.W. Pennington, J. Tytgat, R.S. Norton, Identification, chemical synthesis, structure, and function of a new Kv1 channel blocking peptide from *Oulactis sp*, Pept. Sci. 110 (2018) e24073.

[37] K.A. Elnahriry, D.C.C. Wai, B. Krishnarjuna, N.N. Badawy, B. Chittoor, C. A. MacRaild, B.J. Williams-Noonan, J.M. Surm, D.K. Chalmers, A.H. Zhang, S. Peigneur, M. Mobli, J. Tytgat, P. Prentis, R.S. Norton, Structural and functional characterisation of a novel peptide from the Australian sea anemone *Actinia tenebrosa*, Toxicon 168 (2019) 104–112.

[38] B. Krishnarjuna, P. Sunanda, J. Villegas-Moreno, A. Csoti, G. Panyi Wai, P. Prentis, R.S. Norton, A disulfide-stabilised helical hairpin fold in acrorhagin I: an emerging structural motif in peptide toxins, J. Struct. Biol. 213 (2021) 107692.

[39] K. Sanches, L.M. Ashwood, A.A. Olushola-Siedoks, D.C.C. Wai, A. Rahman, K. Shakeel, M.U. Naseem, G. Panyi, P.J. Prentis, R.S. Norton, Structure-function relationships in ShKT domain peptides: ShKT-Ts1 from the sea anemone *Telmatactis stephensoni*, Proteins 92 (2024) 192–205.

[40] M.L. Mitchell, B.R. Hamilton, B. Madio, R.A.V. Morales, G.Q. Tonkin-Hill, A. T. Papenfuss, A.W. Purcell, G.F. King, E.A.B. Undheim, R.S. Norton, The use of imaging mass spectrometry to study peptide toxin distribution in Australian sea anemones, Aust. J. Chem. 70 (2017) 1235–1237.

[41] L.M. Ashwood, E.A.B. Undheim, B. Madio, B.R. Hamilton, M. Daly, D.A. Hurwood, G.F. King, P.J. Prentis, Venoms for all occasions: the functional toxin profiles of different anatomical regions in sea anemones are related to their ecological function, Mol. Ecol. 31 (2022) 866–883.

[42] B. Madio, S. Peigneur, Y.K.Y. Chin, B.R. Hamilton, S.T. Henriques, J.J. Smith, B. Cristofori-Armstrong, Z. Dekan, B.A. Boughton, P.F. Alewood, J. Tytgat, G. F. King, E.A.B. Undheim, PHAB toxins: a unique family of predatory sea anemone toxins evolving via intra-gene concerted evolution defines a new peptide fold, Cell. Mol. Life Sci. 75 (2018) 4511–4524.

[43] O.D. Tezcan, O. Gozer, Severe toxic skin reaction caused by a common anemone and identification of the culprit organism, J. Travel Med. 22 (2015) 269–271.

[44] C.A. van der Burg, P.J. Prentis, J.M. Surm, A. Pavasovic, Insights into the innate immunome of actiniarians using a comparative genomic approach, BMC Genomics 17 (2016) 850.

[45] J.S. Oliveira, D. Fuentes-Silva, G.F. King, Development of a rational nomenclature for naming peptide and protein toxins from sea anemones, Toxicon 60 (2012) 539–550.

[46] J.M. Surm, H.L. Smith, B. Madio, E.A.B. Undheim, G.F. King, B.R. Hamilton, C. A. van der Burg, A. Pavasovic, P.J. Prentis, A process of convergent amplification and tissue-specific expression dominates the evolution of toxin and toxin-like genes in sea anemones, Mol. Ecol. 28 (2019) 2272–2289.

[47] Z. Xu, Z. Chen, H. Zhang, Adaptation and evolution of the sea anemone *Alvinactis sp.* to deep-sea hydrothermal vents: a comparison using transcriptomes, Ecol. Evol. 12 (2022) e9309.

[48] D. Praher, B. Zimmermann, R. Dnyansagar, D.J. Miller, A. Moya, V. Modepalli, A. Fridrich, D. Sher, L. Friis-Moller, P. Sundberg, S. Foret, R. Ashby, Y. Moran, U. Technau, Conservation and turnover of miRNAs and their highly complementary targets in early branching animals, Proc. Biol. Sci. 288 (2021) 20203169.

[49] C. Camacho, G. Coulouris, V. Avagyan, N. Ma, J. Papadopoulos, K. Bealer, T. L. Madden, BLAST+: architecture and applications, BMC Bioinformatics 10 (2009) 421.

[50] H.L. Smith, D.A. Broszczak, S.E. Bryan, R.S. Norton, P.J. Prentis, Molecular insights into the low complexity secreted venom of *Calliactis polypus*, Genome Biol. Evol. 16 (2024) evae154.

[51] F. Delaglio, S. Grzesiek, G.W. Vuister, G. Zhu, J. Pfeifer, A. Bax, NMRPipe: a multidimensional spectral processing system based on UNIX pipes, J. Biomol. NMR 6 (1995) 277–293.

[52] W.F. Vranken, W. Boucher, T.J. Stevens, R.H. Fogh, A. Pajon, M. Llinas, E.L. Ulrich, J.L. Markley, J. Ionides, E.D. Laue, The CCPN data model for NMR spectroscopy: development of a software pipeline, Proteins 59 (2005) 687–696.

[53] M.W. Maciejewski, A.D. Schuyler, M.R. Gryk, P.R. Moraru II, E.L. Romero, H. R. Ulrich, M. Eghbalnia, F. Livny, J.C. Hoch Delaglio, NMRbox: a resource for biomolecular NMR computation, Biophys. J. 112 (2017) 1529–1534.

[54] D.S. Wishart, C.G. Bigam, J. Yao, F. Abildgaard, H.J. Dyson, E. Oldfield, J. L. Markley, B.D. Sykes, ^{1}H, ^{13}C and ^{15}N chemical shift referencing in biomolecular NMR, J. Biomol. NMR 6 (1995) 135–140.

[55] W. Rieping, M. Habeck, B. Bardiaux, A. Bernard, T.E. Malliavin, M. Nilges, ARIA2: automated NOE assignment and data integration in NMR structure calculation, Bioinformatics 23 (2007) 381–382.

[56] J.P. Linge, S.I. O'Donoghue, M. Nilges, Automated assignment of ambiguous nuclear overhauser effects with ARIA, Methods Enzymol. 339 (2001) 71–90.

[57] Y. Shen, A. Bax, Protein backbone and sidechain torsion angles predicted from NMR chemical shifts using artificial neural networks, J. Biomol. NMR 56 (2013) 227–241.

[58] A. Bhattacharya, R. Tejero, G.T. Montelione, Evaluating protein structures determined by structural genomics consortia, Proteins 66 (2007) 778–795.

[59] M.U. Naseem, G. Gurrola-Briones, M.R. Romero-Imbachi, J. Borrego, E. Carcamo-Noriega, J. Beltran-Vidal, F.Z. Zamudio, K. Shakeel, L.D. Possani, G. Panyi, Characterization and chemical synthesis of Cm39 (a-KTx 4.8): a scorpion toxin that inhibits voltage-gated K^+ channel $K_V1.2$ and small- and intermediate-conductance Ca^{2+}-Activated K^+ channels $K_{Ca}2.2$ and $K_{Ca}3.1$, Toxins 15 (2023) 41.

[60] K. Liu, Soybean trypsin inhibitor assay: further improvement of the standard method approved and reapproved by American Oil Chemists' Society and American Association of Cereal Chemists International (vol 96, pg 635, 2019), J. Am. Oil Chem. Soc. 96 (2019) 635–645.

[61] E.L. Ulrich, H. Akutsu, J.F. Doreleijers, Y. Harano, Y.E. Ioannidis, J. Lin, M. Livny, S. Mading, D. Maziuk, Z. Miller, E. Nakatani, C.F. Schulte, D.E. Tolmie, R. Kent Wenger, H. Yao, J.L. Markley, BioMagResBank, Nucleic Acids Res. 36 (2008) D402–D408.

[62] P.K. Pallaghy, K.J. Nielsen, D.J. Craik, R.S. Norton, A common structural motif incorporating a cystine knot and a triple-stranded β-sheet in toxic and inhibitory polypeptides, Protein Sci. 3 (1994) 1833–1839.

[63] R.S. Norton, P.K. Pallaghy, The cystine knot structure of ion channel toxins and related polypeptides, Toxicon 36 (1998) 1573–1583.

[64] M. Schubert, D. Labudde, H. Oschkinat, P. Schmieder, A software tool for the prediction of Xaa-pro peptide bond conformations in proteins based on ^{13}C chemical shift statistics, J. Biomol. NMR 24 (2002) 149–154.

[65] L. Machado, V.S. De Paula, Y. Pustovalova, I. Bezsonova, A.P. Valente, D. M. Korzhnev, F.C.L. Almeida, Conformational dynamics of a cysteine-stabilized plant defensin reveals an evolutionary mechanism to expose hydrophobic residues, Biochemistry 57 (2018) 5797–5806.

[66] S. Dutta, H.M. Berman, W.F. Bluhm, Using the tools and resources of the RCSB protein data bank, Curr. Protoc. Bioinformatics 1 (2007) 1.9.1–1.9.24.

[67] G. Corzo, J.K. Sabo, F. Bosmans, B. Billen, E. Villegas, J. Tytgat, R.S. Norton, Solution structure and alanine scan of a spider toxin that affects the activation of mammalian voltage-gated sodium channels, J. Biol. Chem. 282 (2007) 4643–4652.

[68] P.K. Pallaghy, B.M. Duggan, M.W. Pennington, R.S. Norton, Three-dimensional structure in solution of the calcium channel blocker ω-conotoxin, J. Mol. Biol. 234 (1993) 405–420.

[69] A. Heitz, L. Chiche, D. Le-Nguyen, B. Castro, ^{1}H 2D NMR and distance geometry study of the folding of *Ecballium elaterium* trypsin inhibitor, a member of the squash inhibitors family, Biochemistry 28 (1989) 2392–2398.

[70] J. Jumper, R. Evans, A. Pritzel, T. Green, M. Figurnov, O. Ronneberger, K. Tunyasuvunakool, R. Bates, A. Zidek, A. Potapenko, A. Bridgland, C. Meyer, S.A. A. Kohl, A.J. Ballard, A. Cowie, B. Romera-Paredes, S. Nikolov, R. Jain, J. Adler, T. Back, S. Petersen, D. Reiman, E. Clancy, M. Zielinski, M. Steinegger, M. Pacholska, T. Berghammer, S. Bodenstein, D. Silver, O. Vinyals, A.W. Senior, K. Kavukcuoglu, P. Kohli, D. Hassabis, Highly accurate protein structure prediction with AlphaFold, Nature 596 (2021) 583–589.

[71] S.T. Henriques, Y.H. Huang, K.J. Rosengren, H.G. Franquelim, F.A. Carvalho, A. Johnson, S. Sonza, G. Tachedjian, M.A. Castanho, N.L. Daly, D.J. Craik, Decoding the membrane activity of the cyclotide kalata B1: the importance of phosphatidylethanolamine phospholipids and lipid organization on hemolytic and anti-HIV activities, J. Biol. Chem. 286 (2011) 24231–24241.

[72] N.L. Daly, S. Love, P.F. Alewood, D.J. Craik, Chemical synthesis and folding pathways of large cyclic polypeptides: studies of the cystine knot polypeptide kalata B1, Biochemistry 38 (1999) 10606–10614.

[73] Y. Moran, H. Weinberger, J.C. Sullivan, A.M. Reitzel, J.R. Finnerty, M. Gurevitz, Concerted evolution of sea anemone neurotoxin genes is revealed through analysis of the *Nematostella vectensis* genome, Mol. Biol. Evol. 25 (2008) 737–747.

[74] M.Y. Sachkova, M. Landau, J.M. Surm, J. Macrander, S.A. Singer, A.M. Reitzel, Y. Moran, Toxin-like neuropeptides in the sea anemone *Nematostella* unravel recruitment from the nervous system to venom, Proc. Natl. Acad. Sci. USA 117 (2020) 27481–27492.

[75] J.M. Surm, Z.K. Stewart, A. Papanicolaou, A. Pavasovic, P.J. Prentis, The draft genome of *Actinia tenebrosa* reveals insights into toxin evolution, Ecol. Evol. 9 (2019) 11314–11328.

[76] E.A. Undheim, M. Mobli, G.F. King, Toxin structures as evolutionary tools: using conserved 3D folds to study the evolution of rapidly evolving peptides, Bioessays 38 (2016) 539–548.

[77] B.G. Fry, K. Roelants, D.E. Champagne, H. Scheib, J.D. Tyndall, G.F. King, T. J. Nevalainen, J.A. Norman, R.J. Lewis, R.S. Norton, C. Renjifo, R.C. de la Vega, The toxicogenomic multiverse: convergent recruitment of proteins into animal venoms, Annu. Rev. Genomics Hum. Genet. 10 (2009) 483–511.

[78] B. Madio, G.F. King, E.A.B. Undheim, Sea anemone toxins: a structural overview, Mar. Drugs 17 (2019) 325.

[79] N.L. Daly, D.J. Craik, Bioactive cystine knot proteins, Curr. Opin. Chem. Biol. 15 (2011) 362–368.

[80] K. Kikuchi, M. Sugiura, T. Kimura, High proteolytic resistance of spider-derived inhibitor cystine knots, Int. J. Pept. 2015 (2015) 537508.

[81] M.L. Colgrave, D.J. Craik, Thermal, chemical, and enzymatic stability of the cyclotide kalata B1: the importance of the cyclic cystine knot, Biochemistry 43 (2004) 5965–5975.

[82] A. Heitz, O. Avrutina, D. Le-Nguyen, U. Diederichsen, J.F. Hernandez, J. Gracy, H. Kolmar, L. Chiche, Knottin cyclization: impact on structure and dynamics, BMC Struct. Biol. 8 (2008) 54.

[83] G. Corzo, N. Gilles, H. Satake, E. Villegas, L. Dai, T. Nakajima, J. Haupt, Distinct primary structures of the major peptide toxins from the venom of the spider *Macrothele gigas* that bind to sites 3 and 4 in the sodium channel, FEBS Lett. 547 (2003) 43–50.

[84] W. Thomsen, M.F. Martin-Eauclaire, H. Rochat, W.A. Catterall, Reconstitution of high-affinity binding of a β-scorpion toxin to neurotoxin receptor site 4 on purified sodium channels, J. Neurochem. 65 (1995) 1358–1364.
[85] N. Zilberberg, O. Froy, E. Loret, S. Cestele, D. Arad, D. Gordon, M. Gurevitz, Identification of structural elements of a scorpion α-neurotoxin important for receptor site recognition, J. Biol. Chem. 272 (1997) 14810–14816.
[86] M. Monastyrnaya, S. Peigneur, E. Zelepuga, O. Sintsova, I. Gladkikh, E. Leychenko, M. Isaeva, J. Tytgat, E. Kozlovskaya, Kunitz-type peptide HCRG21 from the sea anemone *Heteractis crispa* is a full antagonist of the TRPV1 receptor, Mar. Drugs 14 (2016) 229.
[87] J.P. Imredy, R. MacKinnon, Energetic and structural interactions between δ-dendrotoxin and a voltage-gated potassium channel, J. Mol. Biol. 296 (2000) 1283–1294.
[88] O. Froy, N. Zilberberg, D. Gordon, M. Turkov, N. Gilles, M. Stankiewicz, M. Pelhate, E. Loret, D.A. Oren, B. Shaanan, M. Gurevitz, The putative bioactive surface of insect-selective scorpion excitatory neurotoxins, J. Biol. Chem. 274 (1999) 5769–5776.
[89] E.P. Loret, P. Mansuelle, H. Rochat, C. Granier, Neurotoxins active on insects: amino acid sequences, chemical modifications, and secondary structure estimation by circular dichroism of toxins from the scorpion *Androctonus australis* Hector, Biochemistry 29 (1990) 1492–1501.
[90] L. Cohen, I. Karbat, N. Gilles, O. Froy, G. Corzo, R. Angelovici, D. Gordon, M. Gurevitz, Dissection of the functional surface of an anti-insect excitatory toxin illuminates a putative "hot spot" common to all scorpion β-toxins affecting Na^+ channels, J. Biol. Chem. 279 (2004) 8206–8211.